Silicon avalanche photodiodes as detectors for photon correlation experiments

Ekkehard Overbeck and Christian Sinn[a)]
Institut für Physik der Johannes-Gutenberg-Universität, Staudingerweg 7, 55099 Mainz, Germany

Ivo Flammer and Jaro Rička
Institut für Angewandte Physik der Universität Bern, Sidlerstrasse 5, 3012 Bern, Switzerland

(Received 29 October 1997; accepted for publication 13 July 1998)

In view of time correlated photon-counting experiments using wavelengths at the red end of the electromagnetic spectrum, we developed a simple electronic circuit for periodical gated quenching of silicon avalanche photodiodes. We compare the performance of this device with commercially available passive and active quenching modules and a reference photomultiplier. The detection system's nonlinearities, i.e., dead time and afterpulsing, lead to direct and indirect distortions of photocount correlation functions. We characterize this nonlinear behavior by measuring intensity auto- and cross-correlation functions and supply nonlinearity parameters for each of the four detection systems. In addition, transfer functions are given which allow an estimate for the highest count rates accessible for each detection system. © *1998 American Institute of Physics.* [S0034-6748(98)01810-3]

I. INTRODUCTION

Silicon avalanche photodiodes have received growing interest as detectors in photon counting applications because of their smaller size, lower operating voltages, and lower cost compared to photomultiplier tubes.[1] Some of these advantages have been lost in the course of the development of very small photomultiplier modules, which even contain the high voltage supply in a small housing.[2] However, applications demanding high sensitivity at wavelengths towards the red end of the visible electromagnetic spectrum call for the use of photodiodes. Let us recall, for example, *in vivo* light scattering measurements conducted in the human eye[3] or the investigation of highly turbid samples free from distortions of the intensity correlation function due to multiply scattered light.[4]

For single-photon counting, a detector with internal gain is essential because of signal-to-noise considerations. In avalanche photodiodes (APDs) a current avalanche is produced in close analogy to a photomultiplier tube (PMT). This avalanche generates the internal gain not exhibited by ordinary photodiodes. However, in contrast to the photomultiplier tube, the avalanche current has to be terminated by electronic means. The main difference in detectors utilizing APDs for single-photon counting purposes is the way this quenching is performed, i.e., the principle of the electronic circuits used.

We have developed a comparatively simple and inexpensive electronic quenching circuit, which we first will describe in this contribution. We then characterize its performance in comparison with commercially available detectors in view of photon correlation applications. The investigated criteria are the detector sensitivity, dark counts, dead time, and afterpulsing. Direct and indirect effects due to dead time and afterpulsing may strongly distort the temporal photocount correlation function, which is the fundamental quantity in photon correlation experiments.

We will show that despite these nonlinear effects the correlation function can be accurately described for sufficiently large time lags by assuming a third-order dependence of the count rate on the impinging light power.

II. ELECTRONIC PART: HOW TO OPERATE AVALANCHE PHOTODIODES AS SINGLE PHOTON COUNTERS

Recently, a comprehensive and very useful review of quenching circuits for single-photon detection has been published by Cova *et al.*,[5] the notation of which we will follow closely.

APDs differ from ordinary photodiodes as they exhibit internal gain. In the sub-Geiger mode[6] the gain may be approximately 10^2, whereas under Geiger conditions, where the reversed bias supply voltage is chosen above breakdown, a typical gain of 10^6 can be achieved. Any photon absorbed in the semiconductor will generate an electron-hole pair, which is separated and accelerated in the applied electric field. Its kinetic energy will then liberate additional charges, thereby creating a current avalanche. In a free-running avalanche, statistical fluctuations will force the current to zero unless a certain limit (the latch current) is exceeded. Such a self-sustaining avalanche, however, prohibits the detection of any subsequent photons. In order to utilize an APD as a fast and sensitive photon detection system, the termination of the current avalanche is required by reducing the electric field so that the avalanche current falls below the latch current: An efficient quench usually requires a reduction of the electric field below breakdown.

Historically, the first APDs operated as a single-photon counting system were passive quenched devices,[7] in which a

[a)]Author to whom correspondence should be addressed.

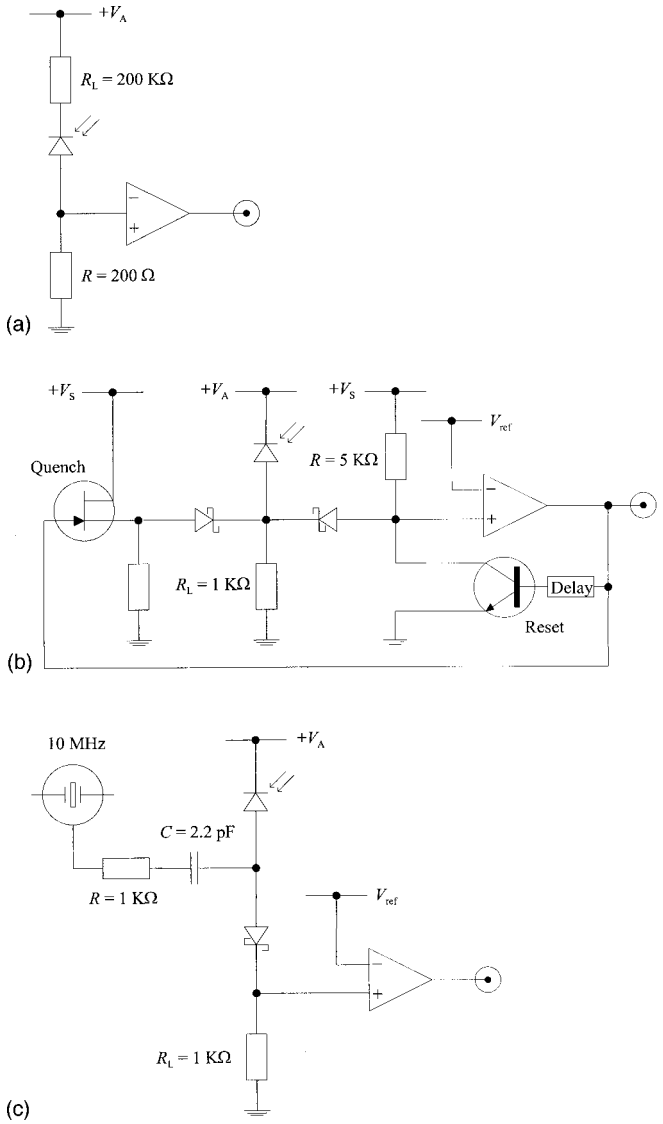

FIG. 1. Scheme of three different electronic quenching circuits. (a) Passive quenching, (b) active quenching, (c) gated quenching.

large load resistor R_L was placed in series with the diode. An electronic scheme for the current-mode output of this most simple electronic circuit is shown in Fig. 1(a). The voltage drop across the load resistor decreases the voltage across the diode so that the current drops below the latch value. Subsequently, the depletion layer is recharged with a time constant $t_r = R_L \cdot C_D$, where C_D is capacitance of the diode plus the stray capacitance. During the recharging time the device is completely unresponsive until the bias voltage is again above breakdown, which typically lasts 200 ns.[8] Subsequently, the sensitivity of the device increases gradually until the bias voltage is fully restored. Accordingly, these devices show no sharply defined dead time. With the typical values $R_L = 200\ \mathrm{k\Omega}$ and $C_D = 2\ \mathrm{pF}$, the time constant $t_r = 400\ \mathrm{ns}$ is comparatively large. This behavior prohibits the use of passively quenched devices for many interesting applications.

A considerable improvement of the performance is achieved by active quenching[9–11] employed today in most of the commercial devices. With this scheme, the leading edge of the current avalanche triggers an active reduction of the bias voltage across the diode; a delay line triggers the reset to the operating value. A schematic layout is shown in Fig. 1(b). This method provides a considerable reduction of the dead time to about 40 ns.

However, there is a third possibility, namely, to quench the diode periodically, independently of whether an avalanche occurred or not.[12,13] The main advantage of this approach is that it leads to a simple and low cost electronic device. The dead time behavior of the gated quenched device is similar to the active quenching: During the second part of the gating period, the bias voltage is held below breakdown and no generated photoelectron is able to initiate a current avalanche. This is in strong contrast to a passive quenching circuit, where in principle a photoelectron is able to start another avalanche with lower current in the course of the diode recharge following the initial one.

Gated circuits will find their main applications with experiments possessing an inherent timing, for example, with time-coded cross-correlation light scattering[14] or experiments utilizing mode-locked lasers.

Our circuit, shown in Fig. 1(c), is in the language of Cova *et al.*, an ac coupled passive gated circuit, quenched by gate termination. The employed thick-junction silicon APD C30921S[15] is preselected for a low dark count rate. We use this light-pipe version, because it is well suited for the connection to a single-mode fiber. The ''reach-through'' structure[16] of this device offers the best commercially available combination of high speed, low noise and capacitance, and short wavelength sensitivity. Still a considerably better performance can be achieved with the Slik-chip,[15,16] which, however, is not available as a separate component.

A convenient feature of our circuit is its flexibility allowing a simple optimization for a specific experimental demand. A crucial task is to optimize the sensitivity while avoiding excessive afterpulsing. The photon detection sensitivity α is given by the product of the quantum efficiency η and the photoelectron detection probability P. While $\eta \approx 70\%$ (at $\lambda = 830$ nm) is the same for any silicon device, the detection probability P increases with U_E, the excess voltage above breakdown. The specified breakdown voltage of the diode is $U_B = 225\ \mathrm{V}$ (at 22 °C); we supply a high voltage $U_A = U_E + U_B$ with $U_E = 2\ \mathrm{V}$, stabilized to within 10 mV. From the data sheet, we then expect a photon detection sensitivity $\alpha = 5\%$ at $\lambda = 830$ nm.

This sensitivity is somewhat low, compared with Slik-chip equipped commercial devices, and therefore one might be tempted to increase the excess voltage U_E. However, increasing U_E would concomitantly lead to stronger afterpulsing. The flow of charges associated with every avalanche fills up impurity levels in the semiconductor band gap. These traps are drained when the supply voltage is risen above breakdown again, thereby leading to delayed avalanches. An increased U_E would liberate charges from even deeper trap levels. This effect can be partly compensated by allowing the trap population to relax during a deep and/or long lasting quench of the supply voltage. We note that this liberation of trapped charges leads to the considerably worse afterpulsing behavior frequently observed with APDs in comparison with PMTs; in addition, the dark count rate is subjected to the same trade-off with U_E as is the afterpulsing probability.

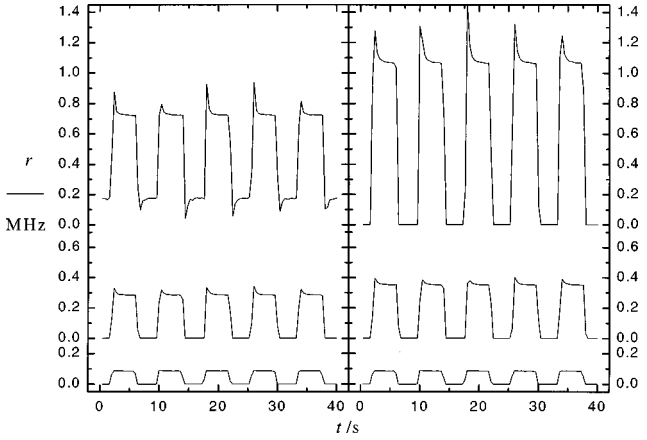

FIG. 2. Measured count rate of the GQ circuit as a function of time, illuminated by a LED chopped with a frequency $\nu=0.12$ Hz. (a) (to the left): Parameter is the applied voltage U_A; from bottom to top: $U_A=\{222,224,226\}$ V. (b) (to the right): Parameter is an increase of the incident light power J, applying $U_A=222$ V; the steady-state count rate $\langle r\rangle$ is, from bottom to top: $\langle r\rangle=\{0.09, 0.35, 1.1\}$ MHz.

With our circuit we supply a 14 V peak-to-peak square pulse of 50 ns symmetric width to the ac coupling capacitor. Due to the voltage division we therefore quench U_A by approximately 7 V with a frequency of 10 MHz.

The breakdown voltage U_B depends strongly on temperature. Since we keep $U_A=U_B+U_E$ constant, any change in the ambient temperature would alter U_E and thus the sensitivity, too. In addition, high count rates lead to energy deposition due to resistive heating, which must be carried off for the same reason. Therefore, the diode can is inserted in a copper block cooled with a Peltier element. The temperature is maintained with the aid of a PID controller at 19 °C with a stability of 0.02 K; at this temperature the break down voltage amounts to $U_B=220$ V. Despite these precautions we observe an overswing of the measured count rate in response to a strong increase of the impinging optical power,[9] as shown in Fig. 2. As the diode is heated at high count rates, it acquires a steady-state temperature due to the heat flow from the chip to the heat sink that is higher than the temperature of the copper block. Accordingly, the plateau value is given by the reduced sensitivity of the diode corresponding to the increase of U_B. When the light is switched off, the diode's high sensitivity is restored with the thermal time constant only.

Figure 2(a) indicates an increase of the thermal overswing with increasing U_A; note that the dark count rate is also increased. Figure 2(b) shows the recordings of the count rate for three different jumps in the incident light power, measured with $U_A=222$ V. Again, a strong overswing is observed above a steady-state count rate of 1 MHz. Although we did not observe any effects due to this overswing in the correlation function, we nevertheless restrict the mean count rates in the present work to less than 1 MHz and keep $U_A=222$ V.

III. THEORETICAL PART: EFFECT OF DEAD TIME AND AFTERPULSING ON CORRELATION FUNCTIONS

The applications of single-photon detectors can be roughly divided into three classes differing in the requirements on the performance of the detector: The first class includes simple low level light detection, which only requires a good sensitivity and a reasonable linearity or simple formulas for nonlinearity corrections. The second class is single-photon timing,[17] which requires a low timing jitter of the output pulse, but dead time and afterpulsing play only a minor role since only the first photoevent following a start trigger is registered. The most stringent requirements on the detector are imposed by the third class of applications encompassing multiphoton timing[18] and photon correlation experiments such as dynamic light scattering (DLS)[19] or fluorescence correlation.[20] Such experiments are particularly sensitive to dead time and afterpulsing. These effects require a thorough consideration and we therefore review the concepts, concentrating thereby on the case of photon correlation in the context of DLS. The quantities that are measured in photon correlation experiments are the photocount correlation functions

$$g_{ij}(\tau)=\frac{\overline{\langle n_i(t)n_j(t+\tau)\rangle}}{\overline{\langle n_i(t)\rangle}\,\overline{\langle n_j(t)\rangle}}, \tag{1}$$

where $n(t)$ represents the number of photoelectron events accumulated within a certain sampling interval $[t,t+t_s]$ at the time instant t. The subscripts stand for one ($i=j=1$) or two detectors ($i=1$, $j=2$) in the case of auto- and cross correlation, respectively. The overbar denotes the averaging with respect to the statistics of the photoevent detection process, whereas the angle brackets represent the temporal average with respect to the fluctuation of the observed light source. For our purpose, it is sufficient to consider thermal fluctuation of classical light, resulting, for example, from Brownian motion of laser illuminated scatterers. With an ideal photon counter the expectation value $\overline{n(t)}$ would be proportional to the expected number of photons impinging on the detector, i.e.,

$$\overline{n}_{\mathrm{id}}(t)=\alpha\int_t^{t+t_s}J(t')dt'\cong\alpha J(t)t_s, \tag{2}$$

where $J(t)$ is the predetection optical signal (expectation of the power operator), α is the photon detection sensitivity of the detector, and t_s the sampling time. In the second part of Eq. (2), we assumed for simplicity that t_s is sufficiently short to regard $J(t)$ as constant. For convenience, we also define the ideal count-rate $r_{\mathrm{id}}(t)=\alpha J(t)$. The second characteristics of an ideal detector is the statistical independence of the detection process in two distinct time intervals, i.e.,

$$\overline{n_{\mathrm{id}}(t)n_{\mathrm{id}}(t+\tau)}=\overline{n_{\mathrm{id}}(t)}\;\overline{n_{\mathrm{id}}(t+\tau)}. \tag{3}$$

For any real detector, the effects of dead time and afterpulsing have to be considered. The distortion of the photocount correlation function by dead time and afterpulsing is twofold. In the first place, one observes the *direct effects*, which are due to a violation of the assumption of statistical independence, Eq. (3). The probability of detecting an event depends on the arrival times of the preceding pulses. Manifestations of this effect are first, the correlation hole for time lags τ smaller than the detectors dead time, and second, the overshooting of the correlation function due to afterpulsing. Di-

rect effects of dead time and afterpulsing limit the shortest time lags τ_1 accessible in a photon correlation experiment.

The second type of distortion due to dead time and afterpulsing are *indirect effects*, which stem from the nonlinearity of the expected count rate with the incident light intensity, i.e., from a violation of Eq. (2). The effect of nonlinearity is particularly severe in DLS experiments, because of the inherently large fluctuations of the predetection signal $J(t)$ to be measured [with DLS, the single time statistics of $J(t)$ is given by an exponential distribution]. Nonlinearity due to dead time results in flattening of the signal peaks and thus in severe distortions of the correlation functions.[21,22]

A rigorous and general *ab initio* derivation of dead time and afterpulsing corrections for the photon correlation functions is a virtually impossible task. The major difficulty is the strong dependence of the effects on the underlying mechanisms, which are rather different for different devices. For example, Schätzel *et al.*[21,22] carried out a thorough analysis of the dead time effect for the two limiting detector models, namely, for paralyzable (extendible dead time) and nonparalyzable detectors, and provided also an interpolation formula for the intermediate situation. However, their treatment assumes a sharply defined dead time period, i.e., the sensitivity $\alpha=0$ during the time interval θ following the primary event, and constant otherwise. This is not applicable for a passively quenched APD, and only an approximation for most devices. A similar situation is encountered with afterpulsing. Burstyn and Sengers[23] analyzed the effect of afterpulsing on photon correlation functions assuming linear behavior of the afterpulsing, i.e., an afterpulsing probability given by the convolution of the train of past events with a certain memory function. In this approximation, the only manifestation of the indirect afterpulsing effect is an enhancement of the sensitivity: α is replaced by $\alpha(1+\gamma)$, where γ is the integral probability for obtaining a photocount due to afterpulsing after an initial pulse. This is not applicable for the APDs, where nonlinear phenomena are involved in generation and recombination of the traps and therefore the afterpulsing probability depends on the count rate in a nonlinear fashion.[18] Adding to these problems the fact that dead time and afterpulsing usually occur simultaneously, there is little hope for a general correction formula.

In our work, we therefore employ a simple practical approach. First of all, we do not attempt a correction for the direct effects. We merely observe whether they are tolerable. If they are not, we employ the cross-correlation scheme: by splitting the received light onto two photon detectors and performing a cross correlation of the two photocount signals, the statistical independence of the detection process in the two distinct systems eliminates any direct effect.[21,24]

However, even when using the cross-correlation scheme, indirect effects remain present and have to be considered for correct data analysis. We employ the simple phenomenological model by Flammer and Rička.[25] This model takes the nonlinearity into account by expanding the expected count rate $r(t)=\overline{n(t)}/t_s$ into a power series in the ideal count rate $r_{\mathrm{id}}(t)=\alpha J(t)$:

$$r(t)=r_{\mathrm{id}}(t)\{1-\theta r_{\mathrm{id}}(t)+\phi\theta^2 r_{\mathrm{id}}^2(t)+O[\theta^3 r_{\mathrm{id}}^3(t)]\}. \quad (4)$$

The correct order of truncation is crucial. It has been shown that the third order in r_{id} is necessary and sufficient for most practically relevant situations.[25] In general, θ and ϕ are regarded as empirical parameters characterizing both the dead time as well as afterpulsing nonlinearity effects. In addition, they would also account for nonlinearity due to variation of the diode's temperature with count rate, if this were to be present. However, these parameters obtain a simple physical meaning in the absence of afterpulsing and thermal nonlinearity: θ is the dead time, or rather an *effective* dead time, when there is a gradual increase of the sensitivity. The so-called updating parameter ϕ can be related directly to Schätzel's model,[21,22] where $\phi=1$ for a nonparalyzable detector and $\phi=1/2$ in the paralyzable limit [this follows from comparing Eq. (4) with Schätzel's Eq. (4) in Ref. 22].

Using Eq. (4) one can calculate the average count rate $\langle r(t)\rangle$ and the photocount correlation functions resulting from a fluctuating predetection signal $J(t)$. Note, however, that the result depends on the statistics of $J(t)$. For example, complex Gaussian statistics of the amplitude of the observed light leads to an exponential power distribution $p(J)=\langle J\rangle^{-1}\exp(-J/\langle J\rangle)$.[26] (This statistics is well realized, for example, by scattering from a suspension of colloidal particles.) In the Gaussian case, as well as in the Poissonian case, $\langle J^2\rangle$ and all higher moments can easily be related to the first moment $\langle J\rangle$. For the Gaussian case, this gives

$$\langle r\rangle=\langle r_{\mathrm{id}}\rangle[1-2\theta\langle r_{\mathrm{id}}\rangle+6\phi\theta^2\langle r_{\mathrm{id}}\rangle^2+O(\theta^3\langle r_{\mathrm{id}}\rangle^3)]. \quad (5)$$

The comparison of this result with Eq. (4) nicely illustrates the severe effect of nonlinearity on strongly fluctuating signals, as already demonstrated in Ref. 22.

Flammer and Rička[25] calculated autocorrelation as well as cross-correlation functions for photon correlation experiments employing contemporary single transverse-mode receivers consisting of a single-mode fiber and a polarizer. Exploiting the fact that the single-mode signal exhibits the same statistical properties as the local intensity of the scattered field, they were able to include the effects of local oscillator and incoherent background (e.g., dark counts or solvent scattering). For the successful application of these correction formulas, an exact determination of the parameters θ and ϕ is crucial. In principle, these parameters can be determined by fitting Eq. (4) or Eq. (5) to an experimental transfer function $\langle r\rangle=f(\langle r_{\mathrm{id}}\rangle)$, measured with a signal obeying the corresponding statistics, e.g., with direct (Poissonian) laser light [Eq. (4)] or (Gaussian) scattered light [Eq. (5)]. However, this procedure requires a calibrated attenuator and is less precise than an alternative procedure proposed in Ref. 25, which does not require the knowledge of $\langle r_{\mathrm{id}}\rangle$. The idea is to measure the normalized variance of the signal fluctuations, i.e., the intercept $\beta=\lim_{\tau\to 0}(\langle\overline{n_i}(0)\overline{n_j}(\tau)\rangle/\langle\overline{n_i}\rangle\langle\overline{n_j}\rangle)-1$ of the photocount autocorrelation function. With Gaussian signal amplitude, we have

$$\beta=1-4\theta\langle r_{\mathrm{id}}\rangle+24\phi\theta^2\langle r_{\mathrm{id}}\rangle^2. \quad (6)$$

Notice the steep decrease of β with increasing input signal, which is governed by the parameters θ and ϕ. The unknown

TABLE I. Performance parameters of the four detection systems investigated. The direct effects of PQa are shown in Fig. 4(a), those of PQb in Fig. 4(b). The afterpulsing probability of GQ is given for a measurement with and without the fast board option.

Detector system	Rel. sensitivity @ λ 514/633 nm	Dark count rate $\langle r_0 \rangle$/Hz	Afterpulsing probability γ(%)	Shortest lag time τ_1/ns
PM	0.14/0.05	16	0.1±0.1	37.5
PQa	1.0/0.9	10	0.9±0.1	1400
PQb			0.6±0.1	1000
AQ	1/1	243	3.5±0.3	600
GQ	0.06/0.08	355	4.6±0.5/0.3±0.1	400

$\langle r_{\mathrm{id}} \rangle$ can be eliminated by reverting the series expansion of Eq. (5).[27] Inserting the second-order result ($\langle r_{\mathrm{id}} \rangle \theta = \theta \langle r \rangle + 2\theta^2 \langle r \rangle^2$) into Eq. (6), one finds

$$\beta = 1 - 4\theta \langle r \rangle + (24\phi - 8)\theta^2 \langle r \rangle^2. \tag{7}$$

Thus, by measuring the dependence of β on $\langle r \rangle$, we can accurately determine θ and ϕ for a specific detector; technical details of the procedure are given in Ref. 25.

IV. EXPERIMENTAL PART: EVALUATION OF THE DETECTORS FOR USE IN PHOTON CORRELATION EXPERIMENTS

A. Photocount correlation functions of laser light

For the determination of the detectors relative sensitivity, they were exposed to the attenuated light of a HeNe laser (λ=632.8 nm), model SP 127.[28] Its cavity length of approximately 1 m results in a mode-beating frequency of 150 MHz, which is too high to be observed with our equipment. The count rate was kept low (at ~100 kHz) to reduce nonlinear effects due to the dead time [Eq. (5)]. In Table I we listed the results for the four detection systems we investigated. Two devices are commercial APD photon counting modules with no setting possibility.[15] PQ, the passively quenched module SPCM-PQ-200, is specified for a dark count rate below 100 Hz and a dead time of 200 ns, whereas the specifications of AQ, the actively quenched SPCM-AQ-131, are a dark count rate below 250 Hz and a dead time of typically 50 ns. Both offer a photon detection sensitivity of $\alpha \approx 50\%$ at λ=830 nm, one order of magnitude higher than that of GQ, our gated quenched device described in Sec. II. This high sensitivity is achieved by working with a comparatively high excess voltage U_E; dark count rate and afterpulsing probability are not degraded because both modules are equipped with the Slik-chip.[15,16] The GQ would achieve a comparable sensitivity ($\alpha \approx 40\%$) by applying $U_E \approx 25$ V. We chose the value of $U_E = 2$ V in order to allow comparison with AQ and PQ as far as dead time, afterpulsing level, and dark count rate are concerned. For PM, the reference photomultiplier, we used an EMI 9863B tube,[29] together with an amplifier/discriminator PM-PD.[30] High voltage and discriminator level were adjusted for minimal afterpulsing probability, leading also to a comparatively low sensitivity.

For the measurement of the direct effects, we measured the photocount autocorrelation function of the HeNe laser source. All detectors, including the homebuilt one, supplied standard TTL output pulses, which were directly fed into an ALV-5000E correlator board[30] with the fast board installed. The fast board extends the correlator's lag times to smaller values; the first two correlator channel octaves have a sampling time of 12.5 ns, followed by 25, 50 ns, and so on. Without the fast board option, the ALV correlator starts its first channel octave with a sampling time of 200 ns. The according channels are measured with a resolution of 25 ns utilizing the fast board. Above a lag time of 1.6 μs the channel separation is the same with and without the fast board option. The correlation functions shown are captured with a single correlator run lasting 100 s. The incident light intensity was suitably attenuated to obtain the same (measured) count rates for every detector. Laser noise was below the detection limit.

Figure 3 shows the autocorrelation functions distorted by the direct effects for the photomultiplier and the AQ device. The photomultiplier [Fig. 3(a)] exhibits only small distortions, as from dead time as well as from afterpulsing. Afterpulsing is only significant in the first correlator channel after the correlation hole. The dead time of the PM detection system is visible as a straight line connecting the first and the second correlator channel at 12.5 and 25 ns, respectively. In contrast, a clear-cut peak is observed in the AQ curve [Fig. 3(b)]. The correlation hole is clearly visible, the dead time is estimated to be approximately $\tau_0 \approx 62.5$ ns, in accordance with the specifications of the manufacturer.

Figure 4(a) shows the respective result for the PQ device we utilize in this contribution. The huge peak at approximately the typical dead time of 200 ns is an artifact of the PQ module of undetermined origin. For comparison, in Fig. 4(b)

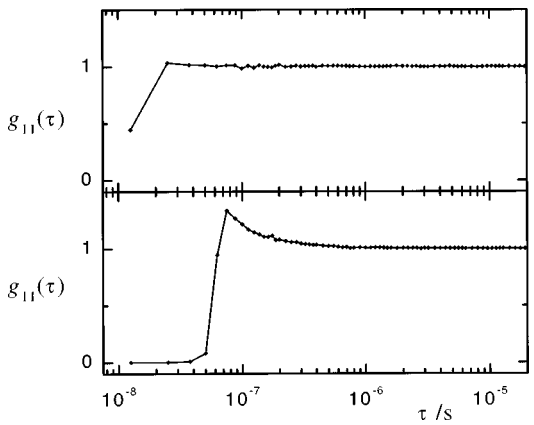

FIG. 3. Photocount autocorrelation functions displaying the direct effect due to detector nonlinearities. The count rates were $\langle r \rangle \approx 100$ kHz in both cases. (a) (top): Photomultiplier plus amplifier/discriminator (PM), (b) (bottom): active quenched APD circuit (AQ).

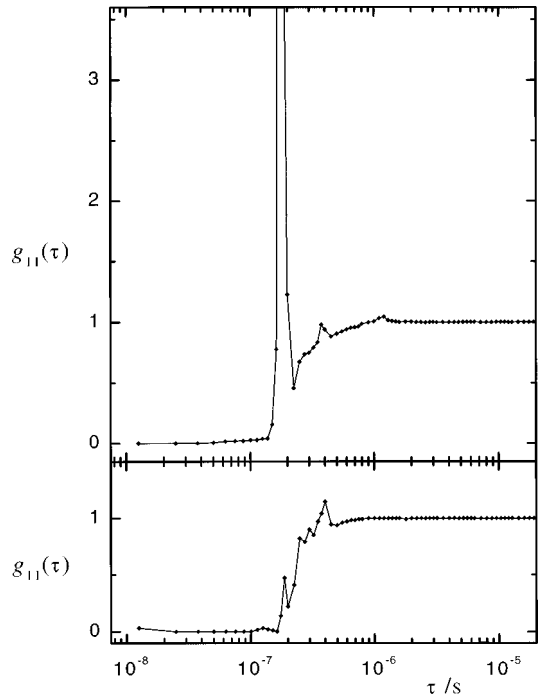

FIG. 4. Photocount autocorrelation functions displaying the direct effect due to detector nonlinearities for the passive quenched APD circuit (PQ). (a) (top): PQ module utilized in this contribution; (b) (bottom): equivalent module with the same specifications as the previous one. The count rates were $\langle r\rangle \approx 100$ kHz in both cases.

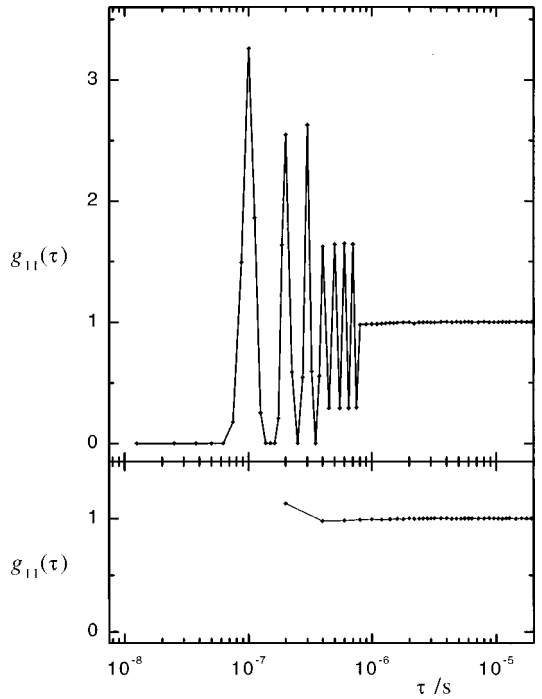

FIG. 5. Photocount autocorrelation functions displaying the direct effect due to detector nonlinearities for the gated quenched APD circuit (GQ). (a) (top): measurement employing the fast board; (b) (bottom): measurement with the conventional correlator board. The count rates were $\langle r\rangle \approx 100$ kHz in both cases.

the correlation function of an equal PQ device is shown, measured two years ago. We note that both correlation functions are quite similar as far as the peak positions are concerned and interpret this as due to a small difference in the typical dead time of the PQ devices, which may originate from slight variations of the diode's stray capacitance or the load resistor. As its dead time is slightly larger, the peak is strongly depressed in the older PQ device. Unfortunately, this module is no longer available in our laboratory, which prohibits us to confirm our speculation. With both modules, the gradually increasing sensitivity of the device following the dead time, as described earlier, leads to the slow increase in the correlation function after the dead time up to lag times of approximately 1 μs. An extrapolation of this course back to $g_{11}(\tau)=0$ yields an estimate for the dead time $\tau_0 = 150-200$ ns.

Figure 5(a) shows the result for the GQ circuit. A conspicuous feature of the correlation function are the triangles reflecting the autocorrelation of the rectangular gate pulses. Their amplitude decreases with increasing lag time, because of the increasing averaging time of the multiple-tau correlator and dephasing of the gating period and the correlator clock. These triangles could be removed by synchronizing the correlator clock with the gate signal, but they disappear anyway when sampling times larger than the detector's quenching period of 100 ns are used [e.g., when the fast board option of our correlator is switched off, cf. Fig. 5(b)]. The maximum dead time is the period from the beginning of the active to the termination of the quenched period, i.e., 100 ns. A peak value of the self-correlating triangles larger than two indicates afterpulsing contributions. If the triangles are removed on the expense of time resolution, we are left with comparatively small afterpulsing effects extending up to a time lag of approximately $\tau_1 = 400$ ns.

As the measure of the afterpulsing probability γ, we determine the excess area over $g_{11}(\tau)=1$, i.e.,

$$\gamma = \sum_{j=j_0}^{j_1} [g_{11}(\tau_j)-1]\langle r\rangle \cdot \tau_j . \tag{8}$$

j is the channel number of the correlator. The summation starts at the edge of the correlation hole (j_0 is the channel number corresponding to τ_0) and is terminated at the first channel j_1, where $g_{11}(\tau_1)$ falls below 1.02. The measurements were performed with a count rate $\langle r\rangle = 100$ kHz in all four cases to ensure comparability; the results are shown in Table I. For PQ, the result is given for both systems mentioned, ignoring the strong peak in Fig. 4(a). For GQ, a value determined from Fig. 5(a) as well as from Fig. 5(b) is given. Unfortunately, the experimental results for γ depend on the time resolution of the experiment as well as on the count rates used. Consequently, in the literature these data differ by orders of magnitude.[7,10,15,16] For photon correlation measurements, however, the first correlator channel j_1 of interest is the one that exhibits no influence of afterpulsing effects. In Table I corresponding τ_1 data are included, obtained by the procedure explained above, which give an estimate for the smallest lag time accessible with the respective detector.

B. Photocount correlation functions of Gaussian light

We illuminated a latex sample with polystyrene spheres of $d = 173$ nm nominal diameter with an Ar^+ laser ($\lambda = 514.5$

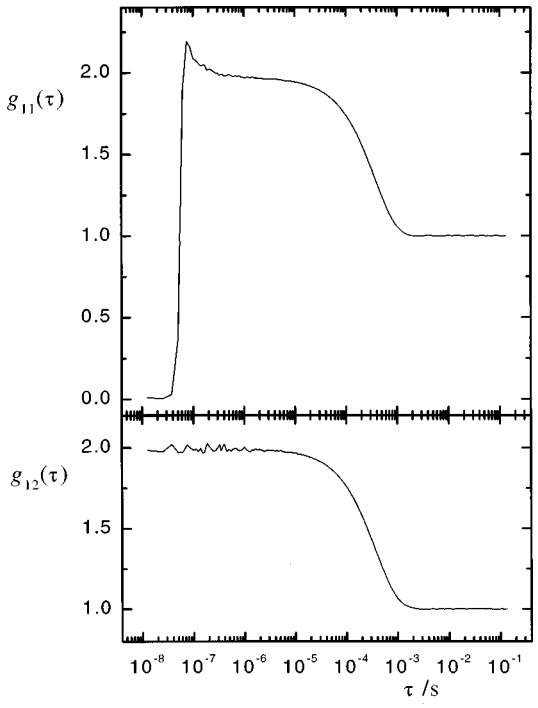

FIG. 6. Photocount correlation functions of the light scattered by a polystyrene latex sample under an angle of 90°, measured with an active quenched APD. (a) Autocorrelation function, the count rate was $\langle r\rangle = 179$ kHz. (b) Cross-correlation function; the count rates were $\langle r\rangle_{AQ} = 182$ kHz and $\langle r\rangle_{PM} = 14$ kHz.

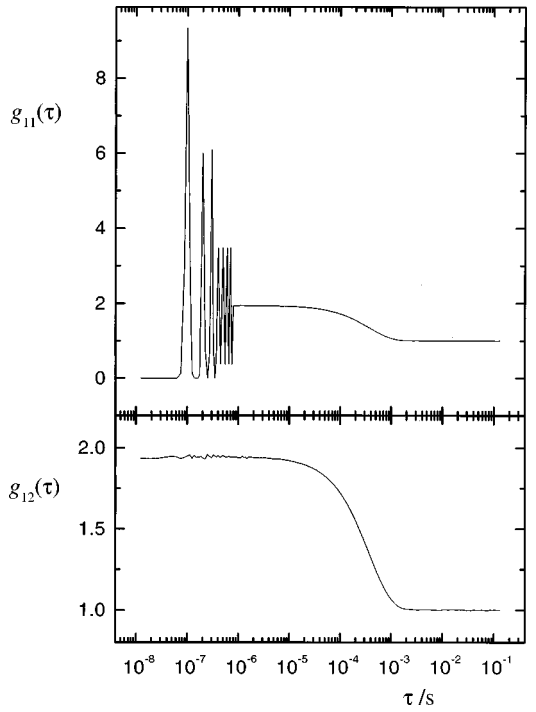

FIG. 7. Photocount correlation functions of the light scattered by a polystyrene latex sample under an angle of 90°, measured with a gated quenched APD. (a) Autocorrelation function, the count rate was $\langle r\rangle = 89$ kHz. (b) Cross-correlation function, the count rates were $\langle r\rangle_{GQ} = 170$ kHz and $\langle r\rangle_{PM} = 170$ kHz.

nm), model Lexel 95;[31] again, the mode beating frequency of the laser is higher than the limiting frequency of the correlator. The sample was held at room temperature and had a very low particle volume fraction of about 10^{-6}. Care was taken that no coherent or incoherent background light contributed to the measured signal. The scattered light was observed under an angle of 90° with a single-mode fiber receiver.

Figure 6(a) shows the autocorrelation function $g_{11}(\tau)$ for the AQ module; direct effects of dead time and afterpulsing are clearly visible. At lag times higher than τ_1, the intercept β of the autocorrelation function amounts almost to one ($\beta = 0.98$), a sign of small indirect effects due to detector nonlinearities at the used count rate of $\langle r\rangle = 179$ kHz. Figure 7(a) shows $g_{11}(\tau)$ for the GQ circuit. After the self-correlating triangles, we obtain an intercept of $\beta = 0.93$, indicating stronger nonlinearity effects as compared to the AQ module. In addition, cross-correlation functions $g_{12}(\tau)$ of the same signals are shown [Figs. 6(b) and 7(b)]. They were obtained by splitting the light path at the end of the receiving single-mode fiber and feeding the light by two multi-mode fibers into the test detector and the reference photomultiplier, respectively. As expected, no reminiscence of the direct effects are observed, i.e., all time lags of the correlation function can be evaluated. The counting noise at small lag times is somewhat larger in Fig. 6(b) than in Fig. 7(b) because of the lower count rate of the PM. Note that the intercept β in Fig. 7(b) is again smaller than the theoretical value of one, as expected, because the indirect effects are present even in the cross correlation. The analysis of the indirect effect on the cross correlation is given in Ref. 25, but the formulas are somewhat lengthy, as both detector nonlinearity parameters contribute, weighted by the respective count rate. The difference in the intercept between AQ and GQ (Figs. 6 and 7), however, is clearly due to the larger dead time parameter of the GQ device.

From the intercept β of the autocorrelation function (again taken at lag times larger than τ_1) as a function of count rate, which is shown in Fig. 8 for all four detection systems, the detector nonlinearity parameters θ and ϕ can be determined as described in Sec. III. The results are listed in Table II together with the dead time τ_0 estimated from the direct effect. We find a reasonable agreement between θ and τ_0, but we keep in mind that the precision of the direct

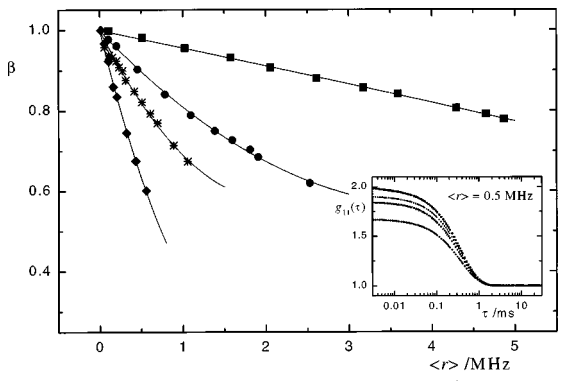

FIG. 8. Intercept β of $g_{11}(\tau)$ of the light scattered by a polystyrene latex sample under an angle of 90° as a function of the count rate $\langle r\rangle$, measured with four different detection systems. The inset shows the respective autocorrelation functions for $\langle r\rangle \approx 0.5$ MHz. The detection systems shown are from top to bottom: PM (squares), AQ (circles), GQ (stars), PQ (diamonds). The drawn lines are the fitted functions according to Eq. (7).

estimation is insufficient for accurate correction of DLS measurement, especially in the presence of an unknown amount of stray light.[25] The measured intercept in the limit of zero count rate increases up to one within 1%, thus justifying the neglect of background contributions and the single-mode assumption for the optical receiver in Sec. III. We note that the intercept can be described within an error below 1% for every detector by including the third order corrections. Higher order corrections become important at count rates higher than those up to which the fit lines are drawn in Fig. 8. On the other hand, below a count rate of $\langle r\rangle \cdot \theta = 0.03$, the highest order term in our calculation amounts to less than 1% (assuming $\phi = 0.5$). As an illustrative example, the intercept measured with AQ can be described by setting $\phi = 0$ up to the comparatively low count rate of $\langle r\rangle = 0.6$ MHz only.

Figure 9 shows the transfer functions according to Eq. (5), obtained from the fitted parameters θ and ϕ. The nonlinearity of all four detector systems is clearly visible, the differences between the detectors arising mainly from their differences in dead time.

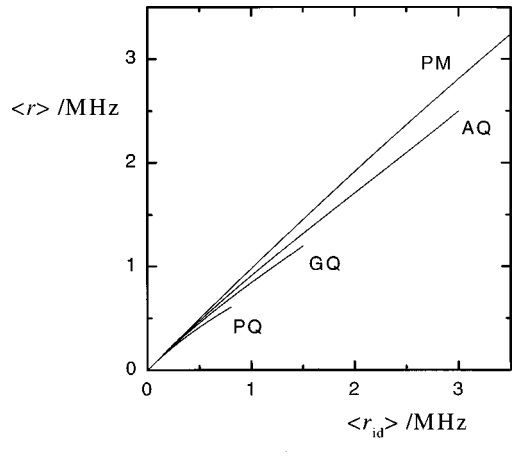

FIG. 9. Transfer functions for Gaussian inputs of the four detection systems, as indicated.

V. DISCUSSION: COMPARISON OF THE AVALANCHE PHOTODIODE DETECTORS INVESTIGATED

Clearly, the best performance, in terms of the sensitivity as well as of the direct or indirect effects of dead time and afterpulsing, is exhibited by the EG&G AQ device. The PQ device from the same manufacturer exhibits the same high sensitivity but the linearity is by comparison poor. An improvement is hardly feasible, which also seems to be the conclusion of the manufacturer, who stopped the production of the device. However, a GQ circuit with a suitably chosen gate period, may be an inexpensive alternative to the commercial AQ module. From Table I it can be seen that with respect to dark count rate, afterpulsing probability and shortest advisable lag time, our GQ circuit and the AQ module exhibit comparable performances. With the available APD chip, this favorable behavior of the GQ circuit can only be achieved at the expense of a strongly reduced sensitivity, which, however, is still comparable with a photomultiplier, and is acceptable in many applications. The sensitivity of the GQ device can be enhanced by increasing the applied voltage, but only at the expense of higher dark count rate and afterpulsing probability. An advantage of the GQ circuit, not yet exploited in the present contribution, is the easy synchronization with an external clock. It would be highly interesting to investigate the performance of the GQ device equipped with an alternative APD, preferably with the EG&G Slik-chip.

TABLE II. Dead time τ_0 estimated from the width of the correlation hole, and detector nonlinearity fitting parameters θ and ϕ according to Eq. (7). The estimated error in θ is 5%, the error in ϕ is 10%.

Detector system	Estimated dead time τ_0 /ns	Dead time parameter θ/ns	Updating parameter ϕ
PM	<12.5	11	0.21
PQ	150...200	213	0.55
AQ	62.5	54	0.71
GQ	50...100	102	0.73

ACKNOWLEDGMENTS

The main experimental part of this work, namely, the gated quenching circuit, was initiated and is based on ideas and suggestions from Klaus Schätzel, who did not live to see the success of his work. We lost, far too soon, an inspiring researcher, good friend, and, last but not least, patient head of the group. E.O. and C.S. acknowledge the support by Thomas Palberg. This work would not have reached the state it did without the continuous assistance, interest, and patience of Hendrik Kuiper from the electronic workshop of the Institute of Physics in Mainz. We learned a lot from him and are grateful for this delightful cooperation. This work was supported by DFG via SFB 262 and Swiss National Foundation. The authors would like to express their warm thanks to the referee for his abundant and pertinent comments and suggestions.

[1] T. Louis, G. H. Schatz, P. Klein-Bölting, A. R. Holzwarth, G. Ripamonti, and S. Cova, Rev. Sci. Instrum. **59**, 1148 (1988).
[2] Hamamatsu Photonics, Iwata-gun, Toyooka-shi, Shimokanzo, Japan.
[3] L. Rovati, F. Frankhauser II, and J. Rička, Rev. Sci. Instrum. **67**, 2615 (1996).
[4] E. Overbeck and Chr. Sinn, J. Mod. Opt. (accepted).
[5] S. Cova, M. Ghioni, A. Lacaita, C. Samori, and F. Zappa, Appl. Opt. **35**, 1956 (1996).
[6] R. G. W. Brown and M. Daniels, Appl. Opt. **28**, 4616 (1989).
[7] R. G. W. Brown, K. D. Ridley, and J. G. Rarity, Appl. Opt. **25**, 4122 (1986).
[8] Li-Qiang Li and L. M. Davis, Rev. Sci. Instrum. **64**, 1524 (1993).
[9] R. G. W. Brown, R. Jones, J. G. Rarity, and K. D. Ridley, Appl. Opt. **26**, 2383 (1987).
[10] A. Spinelli, L. M. Davis, and H. Dautet, Rev. Sci. Instrum. **67**, 55 (1996).
[11] I. Prochazka, K. Hamal, B. Sopko, J. Rička, and M. Höbel, Inst. Phys. Conf. Ser. **126**, 147 (1991).
[12] B. F. Levine and C. G. Bethea, Appl. Phys. Lett. **44**, 553 (1984).
[13] B. F. Levine and C. G. Bethea, Electron. Lett. **20**, 269 (1984).
[14] K. Schätzel, J. Mod. Opt. **38**, 1845 (1991).
[15] EG&G Optoelectronics Canada Ltd., Vaudreuil, Quebec, Canada. The diode chip is the same as in RCA C30902S.
[16] H. Dautet, P. Deschamps, B. Dion, A. D. MacGregor, D. MacSween, R. J. McIntyre, C. Trottier, and P. P. Webb, Appl. Opt. **32**, 3894 (1993).

[17] D. V. O'Connor and D. Phillips, *Time Correlated Single Photon Counting* (Academic, London, 1984).
[18] M. Höbel and J. Rička, Rev. Sci. Instrum. **65**, 2326 (1994).
[19] See, e.g., the contribution by K. Schätzel, in *Dynamic Light Scattering: The Method and Some Applications*, edited by W. Brown (Clarendon, Oxford, 1993).
[20] D. Magde and E. L. Elson, Biopolymers **17**, 29 (1974).
[21] K. Schätzel, Appl. Phys. B: Photophys. Laser Chem. **41**, 95 (1986).
[22] K. Schätzel, R. Kalström, B. Stampa, and J. Ahrens, J. Opt. Soc. Am. B **6**, 937 (1989).
[23] H. C. Burstyn and J. V. Sengers, Phys. Rev. A **27**, 1071 (1983).
[24] F. T. Arecchi, M. Corti, V. Degiorgio, and S. Donati, Opt. Commun. **3**, 284 (1971).
[25] I. Flammer and J. Rička, Appl. Opt. **36**, 7508 (1997).
[26] J. W. Goodman, *Statistical Optics* (Wiley, New York, 1985).
[27] *Handbook of Mathematical Functions*, edited by M. Abramowitz and I. A. Stegun, 9th printing (Dover, New York, 1970), p. 16.
[28] Spectra-Physics Lasers Inc., Mountain View, California.
[29] THORN EMI Electron Tubes Ltd., Ruislip, Middlesex, United Kingdom.
[30] ALV GmbH, Langen, Germany.
[31] Lexel Laser Inc., Milmont Dr., Fremont, California.